INTERNATIONAL JOURNAL FOR NUMERICAL METHODS IN FLUIDS, VOL. 22, 297–311 (1996)

COMPARISON OF NUMERICAL SCHEMES IN LARGE-EDDY SIMULATION OF THE TEMPORAL MIXING LAYER

BERT VREMAN, BERNARD GEURTS AND HANS KUERTEN

Department of Applied Mathematics, University of Twente, PO Box 217, NL-7500 AE Enschede, Netherlands

SUMMARY

A posteriori tests of large-eddy simulations for the temporal mixing layer are performed using a variety of numerical methods in conjunction with the dynamic mixed subgrid model for the turbulent stress tensor. The results of the large-eddy simulations are compared with filtered direct numerical simulation (DNS) results. Five numerical methods are considered. The cell vertex scheme (A) is a weighted second-order central difference. The transverse weighting is shown to be necessary, since the standard second-order central difference (A′) gives rise to instabilities. By analogy, a new weighted fourth-order central difference (B) is constructed in order to overcome the instability in simulations with the standard fourth-order central method (B′). Furthermore, a spectral scheme (C) is tested. Simulations using these schemes have been performed for the case where the filter width equals the grid size (I) and the case where the filter width equals twice the grid size (II). The filtered DNS results are best approximated in case II for each of the numerical methods A, B and C. The deviations from the filtered DNS data are decomposed into modelling error effects and discretization error effects. In case I the absolute modelling error effects are smaller than in case II owing to the smaller filter width, whereas the discretization error effects are larger, since the flow field contains more small-scale contributions. In case I scheme A is preferred over scheme B, whereas in case II the situation is the reverse. In both cases the spectral scheme C provides the most accurate results but at the expense of a considerably increased computational cost. For the prediction of some quantities the discretization errors are observed to eliminate the modelling errors to some extent and give rise to reduced total errors.

KEY WORDS: large-eddy simulation; numerical schemes; mixing layer

1. INTRODUCTION

Large-eddy simulation (LES) of turbulent flow forms a field of intensive research. Whereas direct numerical simulation (DNS) solves all scales present in the flow, LES solves only the large scale directly and models the effect of the small scales, represented by the turbulent stress, with a subgrid model.[1]

For testing subgrid models, two approaches can be distinguished. In *a priori* tests, model predictions and the exact turbulent stress are compared by filtering a velocity field obtained by DNS[2] or experiments.[3] In this approach no actual large-eddy simulations are performed. The other approach is *a posteriori* testing, in which actual large-eddy simulations are performed and the results are compared with experimental results or results from filtered DNS data.[4] Results of *a priori* tests are certainly of some value but require careful interpretation. They often tend to be too pessimistic,[3,5] since low correlations between stresses and predictions do not necessarily lead to poor results when the model is implemented in an actual LES. On the other hand, high *a priori* correlations do not necessarily result in an accurate LES.[6] Therefore, in order to draw conclusions about the performance of a subgrid model, investigation of the behaviour of the model in actual simulations (*a posteriori* tests) is indispensable.

CCC 0271–2091/96/040297–15

Received December 1994
Revised May 1995

In this paper we will focus on *a posteriori* tests of the dynamic mixed model[7,8] in LES of the temporal mixing layer. This model combines a relatively accurate representation of the turbulent stress by the similarity model with a proper dissipation provided by the dynamic eddy viscosity concept. Compared with a wide range of other subgrid models, the dynamic mixed model was observed to produce relatively accurate results.[6,8]

The discrepancies between the results of LES and corresponding DNS or experiments have two sources: shortcomings of the model (modelling errors) and inaccuracies resulting from the numerical approximation of derivatives on a relatively coarse grid (discretization errors). In LES these sources of errors act simultaneously, which complicates *a posteriori* testing, since the separation of the subgrid modelling and numerical effects in the total error is difficult.[3] For LES not only is a variety of subgrid models available,[9] but also various numerical methods can be adopted. In order to appreciate the role of the discretization error, we will compare LES using the dynamic mixed model in combination with five different numerical methods. Furthermore, we will separate the effects of modelling and discretization error by incorporating large-eddy simulations with the same filter width at higher resolution into the tests.

The discretization error depends not only on the numerical method but also on the ratio between the filter width (Δ) and the grid spacing (h). In practice LES is usually performed with $\Delta = h$ (see e.g. References 10 and 11 or $\Delta = 2h$ (see e.g. Reference 12). In most current research the former option is selected, although in References 13 and 14 it was forced that the total simulation error (arising from the modelling and the discretization) was minimal for $\Delta = 2h$. The work in References 13 and 14 is only applicable to schemes that are second-order-accurate in space. In this paper we will revisit this issue and establish the appropriateness of $\Delta = 2h$ for fourth-order and spectral schemes as well.

The tests in this paper are performed for a particular flow: the temporal mixing layer at $M_R = 0{\cdot}2$ and $Re = 50$. The convective Mach number M_R is low, since we do not study compressibility effects here. The effect of compressibility on subgrid modelling has been investigated in Reference 15. The Reynolds number Re is based on half the initial vorticity thickness. It is sufficiently high to allow a mixing transition to small scales as observed in the incompressible simulations in References 16 and 17. On the other hand it is sufficiently low to enable an accurate DNS that resolves all relevant turbulent scales on the computational mesh.

The paper is organized as follows. In Section 2 we present the filtered Navier–Stokes equations, the formulation of the dynamic mixed subgrid model and the numerical schemes. Results are presented in Section 3, which contains the description of the DNS, the comparison of the LES results with filtered DNS data for several numerical schemes and finally the separation between modelling and discretization error effects. Section 4 summarizes our conclusions.

2. MATHEMATICAL FORMULATION

In this section the filtered Navier–Stokes equations to be solved in a large-eddy simulation are presented and the numerical methods are described.

2.1. The filtered Navier–Stokes equations

The partial differential equations which govern a compressible flow are the Navier–Stokes equations representing conservation of mass, momentum and energy. In large-eddy simulation of turbulent flows these equations are filtered in order to reduce the amount of scales to be solved. The filter operation extracts the large-scale part $\bar{f}$ from a flow variable f as follows:

$$\bar{f}(\mathbf{x}) = \int_{\Omega} G_{\Delta}(\mathbf{x} - \mathbf{y}) f(\mathbf{y})\, d\mathbf{y}. \tag{1}$$

Here Ω is the flow domain and Δ denotes the 'filter width' associated with the kernel G_Δ. We will adopt a filter width which does not depend on the position vector $\mathbf{x}$; consequently, the filter operation is a convolution and commutes with spatial derivatives.[18] For compressible flows, Favre[19] has introduced a related filter operation

$$\tilde{f} = \frac{\overline{\rho f}}{\bar{\rho}}, \tag{2}$$

where ρ denotes the fluid density. The filtered Navier–Stokes equations can be written in the form[15]

$$\partial_t \bar{\rho} + \partial_j(\bar{\rho}\tilde{u}_j) = 0, \tag{3}$$

$$\partial_t(\bar{\rho}\tilde{u}_i) + \partial_j(\bar{\rho}\tilde{u}_i\tilde{u}_j) + \partial_i\bar{p} - \partial_j\check{\sigma}_{ij} = -\partial_j(\bar{\rho}\tau_{ij}) + R_i, \tag{4}$$

$$\partial_t\check{e} + \partial_j[(\check{e} + \bar{p})\tilde{u}_j] - \partial_j(\check{\sigma}_{ij}\tilde{u}_i) + \partial_j\check{q}_j = R_e, \tag{5}$$

where the symbols ∂_t and ∂_j denote the partial differential operators $\partial/\partial t$ and $\partial/\partial x_j$ respectively. Furthermore, the summation convention for repeated indices is used. The independent variables t and x_j represent time and the spatial co-ordinates respectively.

Concerning the flow variables, the Favre-filtered velocity vector is denoted by $\tilde{\mathbf{u}}$, while $\bar{\rho}$ is the filtered density and $\bar{p}$ the filtered pressure. Moreover, $\check{e}$ is the total energy density of the filtered variables:

$$\check{e} = \frac{\bar{p}}{\gamma - 1} + \tfrac{1}{2}\bar{\rho}\tilde{u}_i\tilde{u}_i. \tag{6}$$

The viscous stress tensor based on filtered variables, $\check{\sigma}_{ij}$, is defined as

$$\check{\sigma}_{ij} = \frac{\mu}{Re}S_{ij}, \quad \text{with } S_{ij} = \partial_j\tilde{u}_i + \partial_i\tilde{u}_j - \tfrac{2}{3}\delta_{ij}\partial_k\tilde{u}_k, \tag{7}$$

where δ_{ij} is the Kronecker delta and μ is the dynamic viscosity, expressed by Sutherland's law for air as

$$\mu = \tilde{T}^{3/2}\frac{1 + C}{\tilde{T} + C}, \tag{8}$$

with $C = 0{\cdot}4$. In addition, $\hat{\mathbf{q}}$, represents the heat flux vector based on filtered variables, given by

$$\check{q}_j = -\frac{\mu}{(\gamma - 1)RePrM_R^2}\partial_j\tilde{T}. \tag{9}$$

The Favre-filtered temperature $\tilde{T}$ is related to the filtered density and filtered pressure by the ideal gas law

$$\tilde{T} = \gamma M_R^2\frac{\bar{p}}{\bar{\rho}}. \tag{10}$$

These equations have been made dimensionless by introducing a reference length L_R, velocity u_R, density ρ_R, temperature T_R and viscosity μ_R. In addition, γ, the ratio of the specific heats C_P and C_V, and the Prandtl number Pr are given the values $\gamma = 1{\cdot}4$ and $Pr = 1$. The values of the Reynolds number $Re = \rho_R u_R L_R/\mu_R$ and the reference Mach number $M_R = u_R/\sqrt{(\gamma R_g T_R)}$, where R_g is the universal gas constant, are given below.

In this description the left-hand sides of equations (3–5) are the Navier–Stokes equations expressed in the filtered variables $\bar{\rho}, \tilde{u}_j$ and $\bar{p}$. The right-hand sides of the filtered equations are the so-called subgrid terms. The first subgrid term in the momentum equation (4) contains the turbulent stress tensor, defined as

$$\bar{\rho}\tau_{ij} = \overline{\rho u_i u_j} - \overline{\rho u_i}\,\overline{\rho u_j}/\bar{\rho} = \bar{\rho}(\widetilde{u_i u_j} - \tilde{u}_i\tilde{u}_j). \tag{11}$$

The subgrid term R_i results from the non-linearity in the viscous stress tensor. Expressions for the subgrid terms in the energy equation (5), denoted by R_e, can be found in Reference 15. The subgrid terms have to be modelled with subgrid models. In this paper we will adopt the dynamic mixed subgrid model for the turbulent stress tensor τ_{ij} in the momentum equation. The term created by non-linearities in the viscous stress tensor (R_i) can be neglected. Furthermore, no model for the subgrid terms in the energy equation will be assumed. Indeed, *a posteriori* tests have shown that for the mixing layer at low convective Mach numbers the modelling of the sugrid terms in the energy equation has no effect on the large-eddy simulation.[15]

The dynamic mixed subgrid model[7,8] is based on the mixed model formulated by Bardina *et al.*:[20]

$$\bar{\rho}\tau_{ij} = \overline{\overline{\rho u_i}\overline{\rho u_j}/\bar{\rho}} - \overline{\overline{\rho u_i}}\,\overline{\overline{\rho u_j}}/\bar{\rho} - \bar{\rho}C\Delta^2|S|S_{ij}, \tag{12}$$

in which $|S|^2 = \frac{1}{2}S_{ij}S_{ij}$. The first two terms of the model form the similarity model, which is obtained if the definition of $\bar{\rho}\tau_{ij}$ in terms of the unfiltered variables ρ and ρu_i is applied to the filtered variables $\bar{\rho}$ and $\overline{\rho u_i}$. In this way it is assumed that the velocities at different scales give rise to turbulent stresses with similar structures.[21] In the mixed model the similarity model is supplemented with the Smagorinsky eddy viscosity in order to model the discrepancy between the exact turbulent stress and the similarity model. However, like the Smagorinsky model itself, the mixed model is excessively dissipative in the transitional regime and in locations where the flow is laminar.[4] In order to overcome this shortcoming, the dynamic procedure is applied to the mixed model and thus the dynamic mixed subgrid model is obtained. This procedure adjusts the space- and time-dependent model coefficient C to the local turbulent structure of the flow.[22] In order to determine C in the dynamic mixed model, two different formulations have been proposed.[7,8] In this paper we follow the mathematically consistent formulation presented in the latter reference. The dynamic mixed model has been shown to yield accurate results in both *a priori*[15] and *a posteriori* tests.[7,8]

2.2. *Numerical schemes*

Next we present the numerical methods which will be used to solve equations (3–5). The explicit time integration is performed with a compact storage, four-stage Runge–Kutta method with second-order accuracy.[23] In large-eddy simulations with explicit methods, truncation errors resulting from the spatial discretization method appears to be more important than truncation errors resulting from the discretization in time, since the time step determined by the stability restriction of the numerical scheme is considerably smaller than the time scale of the turbulent fluctuations. We will consider five methods for the discretization of the spatial derivatives, presented in Table I. We distinguish between convective and viscous terms. The subgrid terms in the filtered equations are evaluated with the numerical method for the viscous terms. The operators D_j in the table refer to the numerical approximation of the ∂_1-operator for the corresponding method.

In the following the methods A, A′, B, B′ and C are described in more detail. In our description the grid is assumed to be rectangular and uniform with grid spacing h_i in the x_i-direction. Method A is a

Table I. The numerical methods A, A′, B, B′ and C

Method	Convective terms		Viscous terms	
A	D_1	weighted second-order	D_2	second-order
A′	D_1'	second-order	D_2	second-order
B	D_3	weighted fourth-order	D_2	second-order
B′	D_3'	fourth-order	D_2	second-order
C	D_4	spectral	D_4	spectral

robust second-order finite volume method which can easily be formulated for non-uniform grids as well.[24] The discretization for the convective terms is the cell vertex trapezoidal rule, which is a weighted second-order central difference. In vertex (i, j, k) the corresponding operator D_1 for a function f is defined as

$$(D_1 f)_{i,j,k} = (s_{i+1,j,k} - s_{i-1,j,k})/2h_1, \tag{13}$$

with

$$s_{i,j,k} = (g_{i,j-1,k} + 2g_{i,j,k} + g_{i,j+1,k})/4, \qquad g_{i,j,k} = (f_{i,j,k-1} + 2f_{i,j,k} + f_{i,j,k+1})/4.$$

The viscous terms contain second-order derivatives. In method A the viscous stress tensor σ_{ij} and heat flux q_j are calculated in centres of cells. In centre $(i+\frac{1}{2}, j+\frac{1}{2}, k+\frac{1}{2})$ the corresponding discretization $D_2 f$ has the form

$$(D_2 f)_{i+1/2,j+1/2,k+1/2} = (s_{i+1,j+1/2,k+1/2} - s_{i,j+1/2,k+1/2})/h_1, \tag{14}$$

with

$$s_{i,j+1/2,k+1/2} = (f_{i,j,k} + f_{i,j+1,k} + f_{i,j,k+1} + f_{i,j+1,k+1})/4.$$

The divergences of the viscous stress tensor and heat flux are subsequently calculated with the same discretization rule applied to control volumes centred around vertices (i, j, k). Method A is robust with respect to odd–even decoupling. This is illustrated if we consider a function f with $f_{i+1,jk} = -f_{i,j,k}$, called a π-wave in the x_1-direction. The scheme for the viscous terms as described above dissipates such π-waves. Moreover, the discretization of the convective terms with D_1 is such that π-waves in the x_2- and x_3-directions do not appear in $D_1 f$. The standard second-order central difference (labelled as D_1') is obtained if s in equation (13) is replaced by f. In that case, π-waves in the x_2- and x_3-directions do give rise to contributions in $D_1 f$. This argument illuminates why this finite volume method is more robust than the standard second-order central difference and why no artificial dissipation is needed to prevent numerical instability. In method A′ the discretization for the convective terms is the standard second-order central difference, whereas the viscous terms are as in method A.

Using this knowledge, we have constructed a new fourth-order-accurate method which is more robust than the standard five-point fourth-order discretization. Method B employs this discretization for the convective terms, while the viscous terms are still treated as in method A. The corresponding expression for $D_3 f$ has the form

$$(D_3 f)_{i,j,k} = (-s_{i+2,j,k} + 8s_{i+1,j,k} - 8s_{i-1,j,k} + s_{i-2,j,k})/(12h_1), \tag{15}$$

with

$$s_{i,j,k} = (-g_{i,j-2,k} + 4g_{i,j-1,k} + 10g_{i,j,k} + 4g_{i,j+1,k} - g_{i,j+2,k})/16,$$
$$g_{i,j,k} = (-f_{i,j,k-2} + 4f_{i,j,k-1} + 10f_{i,j,k} + 4f_{i,j,k+1} - f_{i,j,k+2})/16.$$

This scheme is conservative, since it is a weighted central difference. The coefficients in the definition for $g_{i,j,k}$ are chosen such that $g_{i,j,k}$ is a fourth-order-accurate approximation to $f_{i,j,k}$ and π-waves in the x_3-direction give no contributions to $g_{i,j,k}$. The definition for $s_{i,j,k}$ has the same properties with respect to the x_2-direction. Consequently, this method is more robust with respect to odd–even decoupling than the standard five-point fourth-order central difference (labelled as D_3'), which is recovered if s in equation (15) is replaced by f. The latter discretization is used for the convective term in method B′, whereas the viscous terms in B′ are as in method B. For convenience we refer to methods B and B′ as fourth-order methods, but we remark that the formal spatial accuracy of the scheme is only second-order owing to the treatment of the viscous terms. However, since the instabilities in the mixing layer

are *convective* instabilities, the convective terms play a more important role than the viscous terms and for this reason it is expected to be sufficient to treat only the convective terms more accurately in order to obtain a more accurate method. Another example of numerical simulations in which the convective terms are treated with a fourth-order-accurate scheme while the viscous terms are treated with a second-order-accurate scheme is found in Reference 11.

Finally, method C is a pseudospectral scheme for the convective and viscous terms. Derivatives in the periodic x_1- and x_3-directions are evaluated using discrete Fourier transforms. Free slip boundaries are imposed in the x_2-direction, which implies that a flow variable is symmetric or antisymmetric at these boundaries. To evaluate derivatives in the x_2-direction, discrete cosine and sine expansions are employed for the symmetric ($\bar{\rho}, \tilde{u}_1, \tilde{u}_3, \check{e}$) and antisymmetric variables ($\tilde{u}_2$) respectively. This spectral method does not dissipate π-waves, which leads to contributions to the so-called 'oddball' wave number. As in Reference 25, the oddball component (π-wave) is explicitly removed at each stage within a time step to prevent numerical instability.

3. RESULTS OF SIMULATIONS

In this section we will present results of large-eddy simulations using the numerical schemes listed in the previous section. The results will be compared with results of filtered direct numerical simulations.

3.1. The DNS results

In order to simulate a three-dimensional temporal mixing layer, we solve the flow equations in a cubic geometry $[0, L] \times [-\frac{1}{2}L, \frac{1}{2}L] \times [0, L]$. Periodic boundary conditions are imposed in the x_1- and x_3-directions, while in the x_2-direction the boundaries are free slip walls, i.e. the normal velocity and the normal derivatives of the density, pressure and tangential velocities are zero. The basic initial velocity profile is the hyperbolic tangent profile $u_1 = \tanh x_2$. The initial temperature profile is obtained from the Busemann–Crocco law[26] and the initial pressure distribution is uniform. The reference length L_R is half the initial vorticity thickness, while the reference density, velocity, temperature and dynamic viscosity are the initial upper stream values. As in other simulations of the three-dimensional mixing layer,[16,17] the length L of the domain is set equal to four times the wavelength of the most unstable mode according to linear stability theory. Superimposed on the mean profile we put a three-dimensional large-amplitude perturbation as described by Sandham and Reynolds.[27] A low convective Mach number is used ($M_R = 0{\cdot}2$) and Re based on half the initial vorticity thickness equals 50.

The DNS database has been obtained by solving the Navier–Stokes equations, without any subgrid model, on a fine grid with 192^3 cells using method B. Visualization of the DNS demonstrates the roll-up of the fundamental instability and successive pairings. Four rollers with mainly negative spanwise vorticity are observed at $t = 20$. After the first pairing ($t = 40$) the flow has become highly three-dimensional. Another pairing ($t = 80$) yields a single roller in which the flow exhibits a complex structure with many regions of positive spanwise vorticity.[28] This structure is an effect of the transition to turbulence which has been triggered by the pairing process at $t = 40$.[16] The simulations are stopped at $t = 100$, since the single roller at $t = 80$ cannot undergo another pairing. The accuracy of the simulation was found to be satisfactory. First, the linear growth rates of the dominant instability modes were captured within 1%. Furthermore, in a simulation on a coarser grid (128^3 cells) very similar results were obtained.

3.2. Comparison of LES results for several numerical schemes

Results from large-eddy simulations will be compared with filtered DNS data. In this work the top-hat filter with filter width Δ is adopted. The turbulent stress tensor resulting from this filter has

appealing algebraic properties.[29] Some simulations have also been performed with the Gaussian filter and only small differences were found.

The large-eddy simulations presented in this subsection have been performed on a grid with 32^3 cells, which is considerably coarser than the DNS grid. The grid spacing of the coarse grid is denoted by h. Since the role of the numerics is influenced by the ratio Δ/h, we will investigate two cases: $\Delta = 2h$ and h. In order to compare the LES and DNS results, the DNS results are filtered on the fine grid. Next, the filtered data are easily obtained on the coarse grid (being a subset of the fine grid) through restriction of the fine grid data. This procedure also provides the initial conditions of the large-eddy simulations. The discrepancy between the LES and filtered DNS results determines the quality of LES; 'perfect' LES results should coincide with the filtered DNS results. As a further point of reference a coarse grid simulation without subgrid model is performed. The influence of a subgrid model is considered to be small if the errors (deviations from the filtered DNS) are comparable with or larger than the errors of the coarse grid simulation without subgrid model. A large difference between the filtered DNS and the coarse grid simulation without subgrid model indicates that there is something to improve upon; the contribution of a subgrid model should be significant.

The LES and filtered DNS will be compared with respect to the time evolution of two global quantities as well as the spatial structure of the turbulent kinetic energy at a fixed time. First, the evolution of the total kinetic energy,

$$E = \int_\Omega \tfrac{1}{2}\bar{\rho}\tilde{u}_i\tilde{u}_i \, \mathrm{d}\mathbf{x}, \tag{16}$$

and the evolution of the momentum thickness,

$$d = \int_{L/2}^{L/2} \langle\bar{\rho}\rangle(1 - \langle\tilde{u}_1\rangle)(1 + \langle\tilde{u}_1\rangle) \, \mathrm{d}x_2, \tag{17}$$

will be considered. The operator $\langle . \rangle$ represents an averaging over the homogeneous directions x_1 and x_3. Since the definition of the momentum thickness employs the mean velocity profile, tests for the momentum thickness quantify the spreading of the mean velocity profile. Furthermore, we will compare the profiles of the turbulent kinetic energy,

$$k(x_2) = \langle(\tilde{u}_i - \langle\tilde{u}_i\rangle)^2\rangle/2. \tag{18}$$

This quantity will be calculated at $t = 70$, which is well beyond the starting point of the mixing transition process but just before the final pairing has been accomplished. The time $t = 70$ is rather arbitrary; it could equally well be $t = 60$ or 80 without altering the conclusions.

In order to investigate the influence of the numerical scheme, we perform large-eddy simulations for the five numerical methods presented in Section 2.2. The simulations with schemes A, B and C appear to be stable, but the standard central differencing methods A′ and B′ give rise to instabilities. The latter methods lead to an excessive small-scale generation ('π-waves') which is not sufficiently suppressed by the molecular and subgrid dissipation. The transverse weighting introduced in schemes A and B is able to prevent the excessive generation of π-waves. Hence LES calculations on coarse grids using central differences can only be performed with the weighting procedure. In the following we only consider results from the simulations with A, B and C.

Figure 1 shows the results for the $\Delta = 2h$ case obtained with A, B and C, together with the results of the filtered DNS and the coarse grid simulation without subgrid model. For the latter simulation, scheme B has been used; scheme A gives comparable results, while the spectral scheme C results in an unstable coarse grid simulation. Figure 1 shows that for all three methods the results of the dynamic mixed model are better than those corresponding to the coarse grid simulation without subgrid model.

The differences caused by changing the numerical method are considerable, although in general smaller than the effect caused by the subgrid model, which is represented by the difference between LES with the dynamic mixed model and the coarse grid simulation without subgrid model. If we compare the results with the filtered DNS, method B gives the best predictions for E, then C and finally A. For the evolution of the momentum thickness, method C clearly gives the best results, then B and then A. With respect to the k profile the three methods provide comparable accuracy. We conclude that for the $\Delta = 2h$ case, LES with a second-order method (A) gives worse results than LES with a higher-

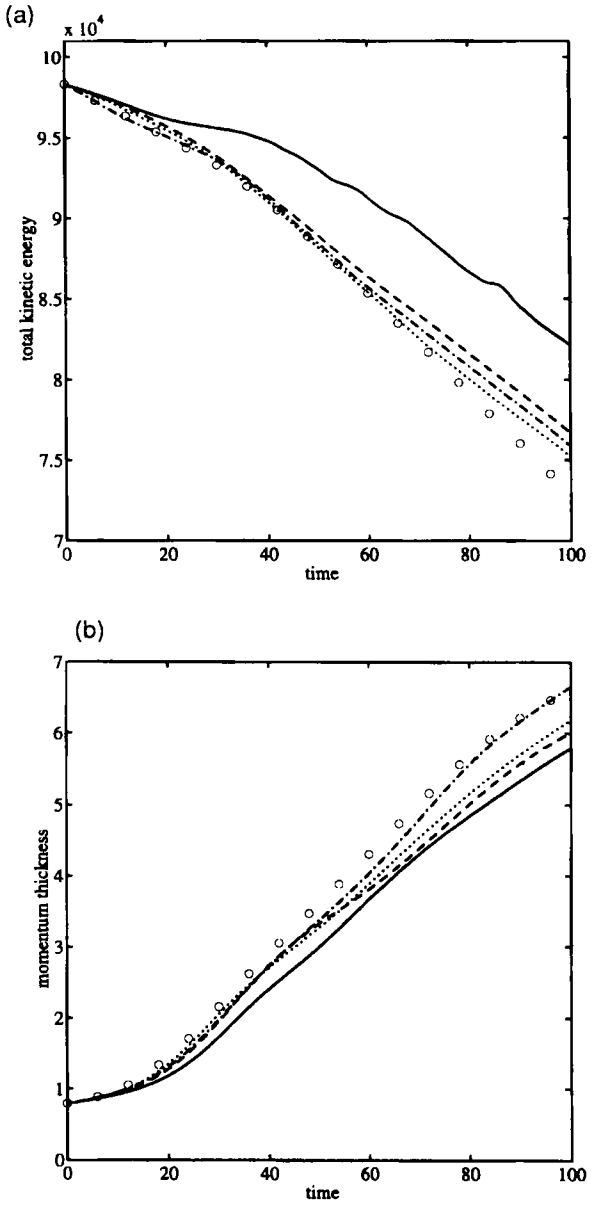

Figure 1. Comparison of numerical methods for $\Delta = 2h$ case: (a) evolution of total kinetic energy; (b) evolution of momentum thickness; Filtered DNS (○); LES with zero model (———); LES with dynamic mixed model using numerical methods A (- - -), B (·····) and C (—·—)

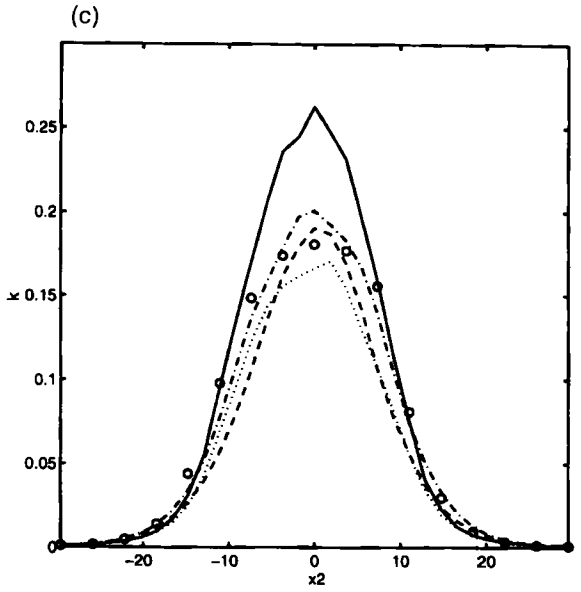

Figure 1. Comparison of numerical methods for $\Delta = 2h$ case: (c) profile of turbulent kinetic energy at $t = 70$. Filtered DNS (○); LES with zero model (———); LES with dynamic mixed model using numerical methods A (- - -), B (·····) and C (–·–)

order method (B or C). For the evolution of the momentum thickness, method C is better than B, but the reverse is true for the total kinetic energy. Furthermore, with respect to computational effort, method C is about five times as expensive as B and seven times as expensive as A. One of the reasons why method C is more expensive is that for numerical stability it requires a convective time step limit which is about three times smaller than method A requires. Therefore, if we take both accuracy and computational cost into account, scheme B is recommended.

The influence of the numerics will certainly be affected by the ration Δ/h. Nest, we will alter this ratio, keeping the grid size h and thus the number of grid points constant, in order to compare results which are obtained with a comparable amount of work. If the ratio Δ/h is decreased for fixed h, more heavily fluctuating fields have to be represented on the same grid, which is expected to give rise to larger discretization errors. Hence in such a case the influence of the numerics will be larger. On the other hand a smaller Δ corresponds to smaller subgrid-scale contributions, which implies that the effect of the subgrid model is expected to be reduced. Probably not only the effect of the subgrid model will become smaller, but the absolute error in the subgrid model as well. Hence for smaller Δ with h constant the discretization error becomes larger and the modelling error becomes smaller. It will be investigated how the sum of these two errors, the total error, behaves. The best Δ/h ratio obviously minimizes the total error in the LES.

In the first part of this subsection we presented results for the $\Delta = 2h$ case; the results for the $\Delta = h$ case are presented in Figure 2 using the same 32^3 grid. The differences caused by changing the numerical method are quite large and in several instances the discrepancy with the filtered DNS is larger than the difference between the coarse grid simulation without subgrid model and the filtered DNS. Comparing the differences with the filtered DNS, scheme A gives the best predictions for the evolution of E, then C and finally B. As far as the momentum thickness d and the k profile are concerned, scheme C gives good results, then A and then B. Hence for the $\Delta = h$ case the best results are obtained with (the most expensive) method C. If we have to choose between the cheaper methods A and B, the lowest-order method A is recommended. This example illustrates that in the $\Delta = h$ case a

second-order method can be preferred over a higher-order method in the class of finite difference methods. Comparing the $\Delta = h$ case (Figure 2) with the $\Delta = 2h$ case (Figure 1), we observe that for each numerical method the curves in Figure 2 are further from the filtered DNS than in Figure 1. Hence the $\Delta = 2h$ case is to be preferred over the $\Delta = h$ case, since it predicts the filtered DNS results more accurately.

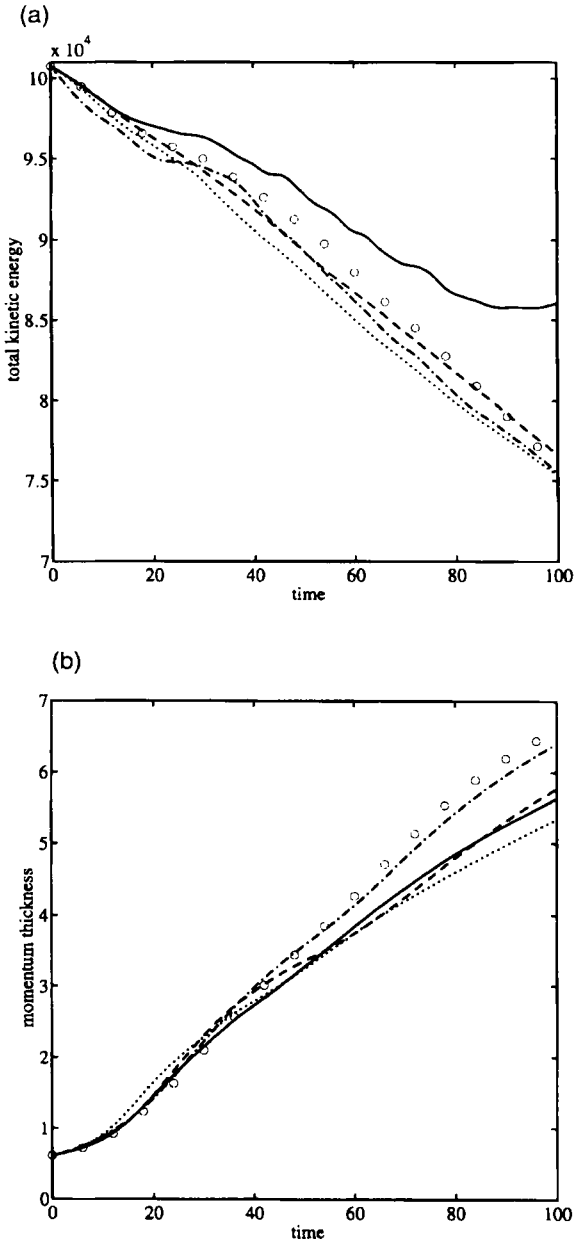

Figure 2. Comparison of numerical methods for $\Delta = h$ case: (a) evolution of total kinetic energy; (b) evolution of momentum thickness; Filtered DNS (○); LES with zero model (———); LES with dynamic mixed model using numerical methods A (- - -), B, (·····) and C (—·—)

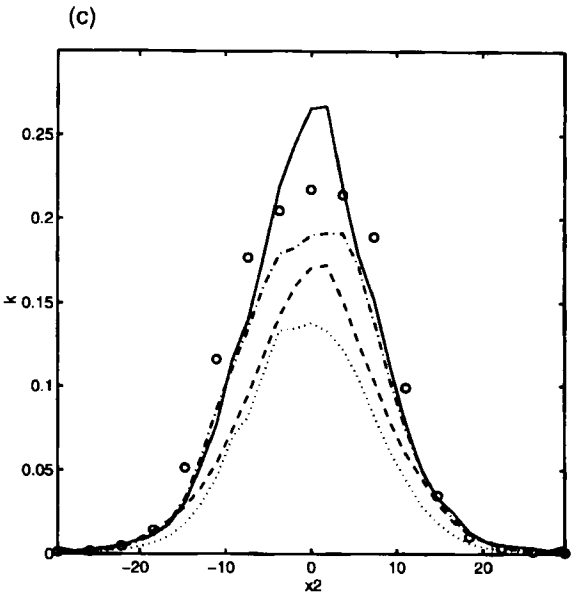

Figure 2. Comparison of numerical methods for $\Delta = h$ case: (c) profile of turbulent kinetic energy at $t = 70$. Filtered DNS (○); LES with zero model (————); LES with dynamic mixed model using numerical methods A (- - -), B (·····) and C (–·–·)

3.3. *Separation between modelling and discretization errors*

In the previous subsection we considered differences between LES and the filtered DNS. These differences we refer to as total errors. They are the sum of two effects: the effect of the modelling error, caused by shortcomings in the subgrid model, and the effect of the discretization error, caused by inaccuracies of the numerical method. In the following we approximately separate these effects. The discretization error in an LES will become smaller if the resolution is increased (h is decreased) while the filter width Δ is kept constant. The discretization error in such a 'fine grid LES' will be considerably smaller than in the original LES. The aim of performing such a fine grid LES is to obtain an LES in which the discretization error effects are small compared with the discretization error effects in the original LES. The difference between those two large-eddy simulations gives an indication of the effect of the discretization error. For the total kinetic energy E we denote the discretization error effect as

$$\epsilon_d(E) = E_{\text{LES}} - E_{\text{fine grid LES}}. \tag{19}$$

We stress that the only difference between the fine grid LES and the original LES is a different grid spacing h; the filter width Δ is the same. Furthermore, since discretization error effects in the fine grid LES are small, the difference between the fine grid LES and the filtered DNS measures the effect of the modelling error:

$$\epsilon_m(E) = E_{\text{fine grid LES}} - E_{\text{filtered DNS}}. \tag{20}$$

The total error is the sum of these two contributions:

$$\epsilon_t(E) = \epsilon_d(E) + \epsilon_m(E) = E_{\text{LES}} - E_{\text{filtered DNS}}. \tag{21}$$

Using equations (19)–(21) allows for an approximate separation of the different sources of error, provided that the discretization error in the fine grid LES is considerably smaller than the discretization error and the modelling error itself in the original LES. Note that $\epsilon_d(E)$ and $\epsilon_m(E)$ are not identical with

the discretization error and the modelling error respectively; they only represent the effect of the discretization or modelling error in E. A small effect of an error in E, for example, does not necessarily imply that the error itself, as it appears on the tensor or vector levels in the filtered Navier–Stokes equations, is small.

Next, we will calculate these errors for the original LES on the 32^3 grid with $\Delta = 2h = L/16$. The corresponding fine grid LES has been performed on a grid with 64^3 points. The ratio between Δ and

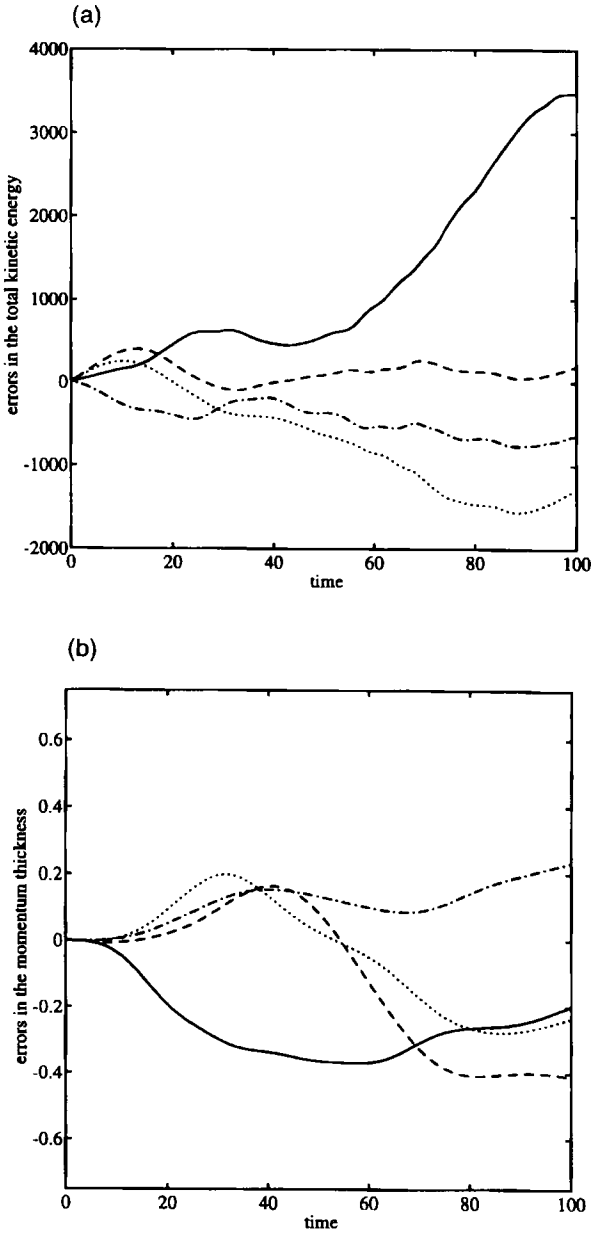

Figure 3. Modelling error effects (————) and discretization error effects for numerical methods A (- - -), B (·····) and C (– · – ·) for LES with $\Delta = 2h$. Errors in (a) evolution of total kinetic energy, (b) evolution of momentum thickness

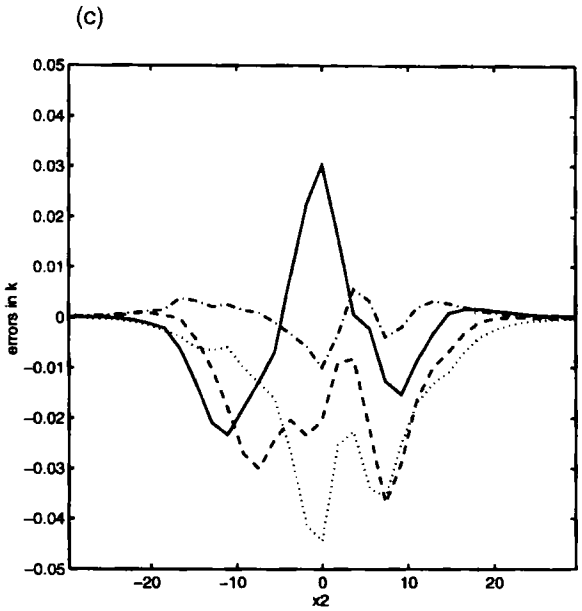

Figure 3. Modelling error effects (————) and discretization error effects for numerical methods A (- - -), B (·····) and C (- · - ·) for LES with $\Delta = 2h$. Errors in (c) profile of turbulent kinetic energy at $t = 70$

the grid spacing in the fine grid LES hence equals 4. This ratio is quite large, which implies that the fields are smooth on the grid scale. Thus the discretization error in such an LES will be considerably smaller than in a DNS with the same resolution. The quantities ϵ_d and ϵ_m are shown in Figure 3. For the evolution of E (Figure 3(a)) the discretization error effects are smaller than the modelling error. The second-order scheme A is observed to give the smallest discretization error effect. It has to be noticed that this does not imply that the discretization error itself is small, but only its effect on the evolution of the total kinetic energy. For schemes B and C the discretization error and modelling error effects have opposite signs, which implies that the discretization error assists the subgrid model in the representation of this quantity: the total error is smaller than the modelling error. For the momentum thickness (Figure 3(b)) the discretization error effects of methods A, B and C and the modelling error effect are of the same order of magnitude. The reason for the good results produced by the spectral scheme is that the discretization error effect is opposite to the modelling error effect during the whole simulation and consequently the total error is considerably lower than the modelling error. Schemes A and B assist the subgrid model only until $t = 50$. After $t = 50$ both schemes increase the total error, but scheme A yields a larger error than the higher-order scheme B. These observations suggest that for the spectral scheme an improvement in the subgrid model (decrease in the modelling error) is expected to give worse results, since the total error will increase, while for schemes A and B an improvement in the model will provide better results after $t = 50$. With respect to the k profile (Figure 3(c)) the discretization error for scheme C gives rise to smaller differences than for schemes A and B. Thus we have observed that the effects of the discretization error are often comparable with the effects of the modelling error. In some instances the discretization error partially cancels the modelling error, which implies that grid refinement will not necessarily give rise to smaller total errors.

In this subsection we have presented results for the $\Delta = 2h$ case. A similar separation of error effects for the $\Delta = h$ case showed that the discretization error effects were larger than in the $\Delta = 2h$ case while the modelling error effects were smaller. This behaviour was to be expected, since a decrease in Δ, with

h kept constant, gives a more fluctuating field leading to less accurate approximations of derivatives, whereas on the other hand the subgrid contributions become smaller, leading to a smaller modelling error. In fact, discretization errors were observed to dominate over modelling errors in the $\Delta = h$ case and consequently further effort to improve the subgrid model does not necessarily lead to improved predictions. *A priori* tests have predicted a similar behaviour.[28,30]

4. CONCLUSIONS

In this paper we have presented *a posteriori* tests of large-eddy simulations of the temporal mixing layer using the dynamic mixed subgrid model in combination with several numerical methods. The numerical methods used were second-order central differences (A weighted and A′ standard), fourth-order central differences (B weighted and B′ standard) and a spectral method (C). Simulations with A′ and B′ turned out to be unstable owing to excessive small-scale generation. The weighting in A and B thus proved to be essential in order to obtain stable calculations.

Employing methods A, B and C, we have compared the cases $\Delta = 2h$ and h. In the $\Delta = 2h$ case the use of a high-order finite difference or a spectral scheme is suggested, while in the $\Delta = h$ case a lower-order finite difference or a spectral scheme has to be preferred. In both cases the spectral scheme gives somewhat better results than the finite difference schemes, but it is also considerably more expensive with respect to computational effort. Taking this into account, scheme B is most efficient. From the comparision of the $\Delta = 2h$ and h cases with respect to total errors (differences from the filtered DNS), we conclude that the former case has to be preferred. It should be noticed that $\Delta = 2h$ does not imply an increased computational cost compared with $\Delta = h$, because only Δ is varied, while h is the same in both cases.

Finally, we have proposed a procedure to separate the effects of discretization and modelling error in the large-eddy simulations. For the $\Delta = 2h$ case the discretization error effects are smaller than or comparable with the modelling error. Furthermore, the discretization error does not always decrease the accuracy; sometimes it assists the subgrid model and thus reduces the total error.

ACKNOWLEDGEMENTS

The time for the computations was provided by the Stichting Nationale Computerfaciliteiten (National Computing Facilities Foundation, NCF), which is financially supported by the Nederlandse Organisatie van Wetenschappelijk Onderzoek (Netherlands Organization for Scientific Research, NWO).

REFERENCES

1. R. S. Rogallo and P. Moin, 'Numerical simulation of turbulent flows', *Ann. Rev. Fluid Mech.*, **16**, 99 (1984).
2. R. A. Clark, J. H. Ferziger and W. C. Reynolds, 'Evaluation of subgrid-scale models using an accurately simulated turbulent flow', *J. Fluid Mech.*, **91**, 1 (1979).
3. C. Meneveau, 'Statistics of turbulence subgrid-scale stresses: necessary conditions and experimental tests', *Phys. Fluids*, **6**, 815 (1994).
4. U. Piomelli, T. A. Zang, C. G. Speziale and M. Y. Hussaini, 'On the large-eddy simulation of transitional wall-bounded flows', *Phys. Fluids A*, **2**, 257 (1990).
5. W. C. Reynolds, 'The potential and limitations of direct and large eddy simulations', in J. L. Lumley (ed.), *Whither Turbulence? Turbulence at Crossroads*, Springer, Berlin, 1990, p. 313.
6. B. Vreman, 'Direct and Large-Eddy Simulation of the compressible turbulent mixing layer', Ph. D. Dissertation, University of Twente, Enschede, 1995.
7. Y. Zang, R. L. Street and J. R. Koseff, 'A dynamic mixed subgrid-scale model and its application to turbulent recirculating flows', *Phys. Fluids A*, **5**, 3186 (1993).
8. B. Vreman, B. Geurts and H. Kuerten, 'On the formulation of the dynamic mixed subgrid-scale model', *Phys. Fluids*, **6**, 4057 (1994).

9. P. Moin and J. Jimenez, 'Large eddy simulation of complex turbulent flows', *Proc. AIAA 24th Fluid Dynamics Conf.*, Orlando, FL, 1993, AIAA, New York, 1993.
10. J. W. Deardorff, 'On the magnitude of the subgrid scale eddy viscosity coefficient', *J. Comput. Phys.*, **7**, 120 (1971).
11. X. Normand and M. Lesieur, 'Direct and large-eddy simulations of transition in the compressible boundary layer', *Theor. Comput. Fluid Dyn.*, **3**, 231 (1992).
12. T. A. Zang, R. B. Dahlburg and J. P. Dahlburg, 'Direct and large-eddy simulations of three-dimensional compressible Navier–Stokes turbulence,' *Phys. Fluids A*, **4**, 127 (1992).
13. M. D. Love, 'Subgrid modelling studies with Burgers' equation', *J. Fluid Mech.*, **100**, 87 (1980).
14. K. Kwak, W. C. Reynolds and J. H. Ferziger, 'Three-dimensional time dependent computation of turbulent flow', *Stanford University Rep. TF-5*, 1975.
15. A. W. Vreman, B. J. Geurts and J. G. M. Kuerten, 'Subgrid-modelling in LES of compressible flows', in P. R. Voke, L, Kleiser and J. P. Chollet (eds), *Direct and Large Eddy Simulation I*, Kluwer, Dordrecht, 1994, p. 133.
16. R. D. Moser and M. Rogers, 'The three-dimensional evolution of a plane mixing layer: pairing and transition to turbulence', *J. Fluid Mech.*, **247**, 275 (1993).
17. P. Comte, M. Lesieur and E. Lamballais, 'Large and small-scale stirring of vorticity and a passive scalar in a 3D temporal mixing layer', *Phys. Fluids A*, **4**, 2761 (1992).
18. B. Geurts, B. Vreman and H. Kuerten, 'Comparison of DNS and LES of transitional and turbulent compressible flow: flat plate and mixing layer', *Proc. 74th Fluid Dynamics Panel and Symp. on Application of DNS and LES to Transition and Turbulence*, Crete, AGARD Conference Proceedings 551, 5.1–14, 1994.
19. A. Favre, 'Turbulence: space–time statistical properties and behavior in supersonic flows', *Phys. Fluids*, **26**, 2851 (1983).
20. J. Bardina, J. H. Ferziger and W. C. Reynolds, 'Improved turbulence models based on LES of homogeneous incompressible turbulent flows', *Department of Mechanical Engineering Rep. TF-19*, Stanford University, 1984.
21. S. Liu, C. Meneveau and J. Katz, 'On the properties of similarity subgrid-scale models as deduced from measurements in a turbulent jet', *J. Fluid Mech.*, **275**, 83 (1994).
22. M. Germano, 'Turbulence: the filtering approach', *J. Fluid Mech.*, **238**, 325 (1992).
23. A. W. Vreman, B. J. Geurts, J. G. M. Kuerten and P. J. Zandbergen, 'A finite volume approach to large eddy simulation of compressible, homogeneous, isotropic, decaying turbulence', *Int. j. numer. methods fluids*, **15**, 799 (1992).
24. H. Kuerten, B. Geurts, J. van der Burg, B. Vreman and P. Zandbergen, 'Development and applications of a 3D compressible Navier–Stokes solver', *Proc. Int. Conf. on Numerical Methods in Fluid Dynamics*, eds. M. Napolitano and F. Sabetta (Springer-Verlag, Berlin), 529–533 (1993).
25. N. D. Sandham and W. C. Reynolds, 'A numerical investigation of the compressible mixing layer', *Department of Mechanical Engineering Rep. TF-45*, Stanford University, 1989.
26. S. A. Ragab and J. L. Wu, 'Linear instabilities in two-dimensional compressible mixing layers', *Phys. Fluids A*, **1**, 957 (1989).
27. N. D. Sandham and W. C. Reynolds, 'Three-dimensional simulations of large eddies in the compressible mixing layer', *J. Fluid Mech.*, **224**, 133 (1991).
28. B. Vreman, B. Geurts and H. Kuerten, 'A priori tests of large eddy simulation of the compressible plane mixing layer', *J. Eng. Math.* **29**, 299 (1995).
29. B. Vreman, B. Geurts and H. Kuerten, 'Realizability conditions for the turbulent stress tensor in large eddy simulation', *J. Fluid Mech.*, **278**, 351 (1994).
30. B. Vreman, B. Geurts and H. Kuerten, 'Discretization error dominance over subgrid-terms in large eddy simulation of compressible shear layers in 2D', *Commun. numer. methods eng.*, **10**, 785 (1994).